Hindawi
Complexity
Volume 2020, Article ID 1492340, 13 pages
https://doi.org/10.1155/2020/1492340

Research Article

Study on Intelligent Compaction-Equipment Logistics Scheduling and Propagation Characteristics of Vibration Wave in Nonlinear Systems with Multistability Based on Field Test

Yixuan Han,[1] **Changwei Yang**,[2] **Degou Cai**,[3] **Hongye Yan**,[3] **and Hailing Zeng**[3]

[1]*Beijing Jiaotong University, 100044 Beijing, China*
[2]*Southwest Jiaotong University Sichuan, 610031 Chengdu, China*
[3]*Railway Engineering Research Institute,*
China Academy of Railway Sciences China Academy of Railway Sciences Corporation Limited, 100044 Beijing, China

Correspondence should be addressed to Changwei Yang; yangchangwei56@163.com

Received 28 January 2020; Accepted 9 March 2020; Published 10 April 2020

Guest Editor: Shao-Bo He

The equipment scheduling and propagation characteristics of vibration wave from vibratory roller ⟶ filling material nonlinear systems with multistability are the core problems of subgrade intelligent construction technology, and the logistics scheduling of the equipment is directly related to the construction efficiency. Aiming at the shortages, one typical subgrade located at the Gu'an station of Beijing-Xiong'an city railway is selected to research and finish the field tests; some findings are shown as follows: first, some valuable suggestions about the logistics scheduling of intelligent equipment are proposed, which can break the barriers between the organizations and improve construction efficiency; second, when the vibration wave propagates from the vibratory roller ⟶ surface of filling material ⟶ different buried depths of filling material, the peak acceleration of vibration wave gradually decreases and is hyperbolic distribution approximately. At the same time, the sensitive of attenuation is shown as follows: $Z<X\approx Y$, and the critical depth of vibration energy propagation is about 1.0 m. At the same time, the peak acceleration of vibration wave at the interface of different filling material layers exists in steps and is "side clock" distribution approximately with the increase in buried depth. Third, in the propagation process, with the increase in buried depth, the amplitude of fundamental, primary, secondary, until fifth harmonics decreases exponentially ($R^2>0.9$), and the concrete functional relationship among different amplitudes of harmonics can be summarized as $y = Ae^{-BX}$; fourth, the vibration energy is mainly concentrated near 10–30 Hz in the vibratory roller, but when the vibration wave propagates from vibratory roller⟶filling material, the vibration energy gradually decreases with the increase in depth, and the marginal spectrum gradually changes from one peak to two peaks, that is, 30–50 Hz and 50–100 Hz; fifth, the vibration energy in the vibrational wheel is distributed averagely in the compaction process, and the effective compaction time is two seconds, which will be helpful for revealing the propagation characteristics of vibration wave, optimizing the compaction quality control models and providing some support for the development of intelligent compaction theory of railway subgrade.

1. Introduction

China has built the world's largest high-speed rail network whose operating mileage reaches 22,000 kilometers and it will be expected to reach 38,000 kilometers in 2030, which will form a high-speed railway network with "eight-vertical and eight-horizontal" as the main channel. The ratio of length of subgrade to total mileage of high-speed railway is more than 30%, which has been an important part of railway infrastructure and the basis for carrying the track structure and trains. In recent years, intelligent compaction technology [1–3] is more and more widely used in practical projects, such as Jingxiong high-speed railway.

Significant engineering achievements have been made in terms of intelligent compaction, but its research on the basic theory has just started; the propagation characteristics of

vibration wave in the compaction process are still not clear enough, and a lot of research studies mainly focus on numerical simulation, theoretical analysis, and laboratory test [4–11] [12].

At the same time, the recent research focuses on two aspects, such as time domain and frequency, but there are little studies on the joint time-frequency domain. However, the vibration wave is a complex nonlinear signal; amplitude and frequency of the vibration gradually change with time, which will affect the reasonability of analysis results if it is analyzed from the time domain or the frequency domain alone. Therefore, the propagation characteristics of vibration wave should be studied from time domain, frequency domain, and joint time-frequency domain by some new signal analysis technology.

Based on this, one typical subgrade section of Beijing-Xiong'an Railway in Gu'an Station is selected to finish the field test, and the intelligent compaction and the logistics scheduling of equipment used in the typical subgrade section are introduced briefly. And then, some valuable test data are used to study the propagation characteristics among soil layers in different depths during the vibration compaction process from time domain, frequency domain, and joint time-frequency domain by Hilbert–Huang transform, which will be helpful for optimizing the compaction quality control models and providing some support for the development of intelligent compaction theory of railway subgrade.

2. Intelligent Compaction and Equipment Deployment Technology

Subgrade intelligent compaction technology mainly integrates automatic monitoring and control, satellite positioning, and information management, as shown in Figure 1.

2.1. Intelligent Compaction Technology. During the construction process, the vibration characteristics of compaction machinery and the compressed filling material are collected in real time by control system, and the main parameters of vibratory roller are continuously adjusted based on the collected information which can reflect the compaction quality in order to optimize compaction and meet the required conditions, such as vibration amplitude, frequency, excitation force, and walking speed. At the same time, the satellite positioning system can accurately determine the position of vibratory roller and feedback the parameters such as modulus, stiffness, and resistance, which is directly related to the compaction quality of filling material to the control system in real time, so as to identify weak areas of subgrade compaction, and then take targeted remedial measures.

2.2. Logistics Scheduling of Intelligent Equipment. In actual operations, the logistics scheduling of intelligent equipment by relevant departments is still in a backward stage. In the construction, because of the lack of modern logistics management knowledge, the integration level in the current construction departments is low, and the management implementation is weak so that the relevant departments often have low utilization rates of resources such as distribution of idle equipment, operations of smart rollers, and dispatch of materials such as machinery and equipment. Aiming at this practical operation problem, this article proposes a scientific logistics scheduling management method. The key to effective scheduling and configuration of intelligent vibratory rollers and other equipment is the establishment of tacit cooperation between all parties, including numerous suppliers, different contractors, and information supporters, connected with the construction project. Due to the particularity of project construction, a temporary and high-efficient material scheduling center should be established, and the collaboration of different organizations is supported by a cross-organizational information platform, as shown in Figure 2.

In the organizational logistics scheduling network, the coordination mechanism is similar to the supply chain network, that is, "To be flexible and rigidly both" [13]. First, each organization node should establish a trusting and harmonious organizational environment. Second, the authority of each organization should be appropriately decentralized; meanwhile, the penetration and connection between different organization subjects should be strengthened via various levels of communication, including information platforms and social network. Third, cross-organizational contracts and agreements in the organizational logistics scheduling network should be finished. Fourth, establishing a sophisticated talent selection system and completing the assessment system are extremely necessary, where both valuing practical skills and academic qualifications, rather than considering merely one.

Based on this, the barriers between the organizations can be broken, completely changing the state of "a pool of standing water" of important materials. Relying on a fast and efficient organizational logistics scheduling network, materials and information flows can quickly transmit and respond between nodes, becoming "live water" where there is demand, and other nodes respond quickly. Whether it is the contradiction between subjective organizations or the contradiction that too many sudden factors cause the failure of resource allocation, it can be solved fundamentally.

3. Test Design

The test site is located in the subgrade section about 200 m by 100 m near the Gu'an Station of the Beijing-Xiong'an Intercity Railway as the test section, as shown in Figure 3. The whole height compacted filling is 1.5 m, which is divided into five layers. The subgrade filling material is the AB group coarse breccia, which is the mixture of A group material and B group material, and the concrete parameters are regulated in detail in the ≪high-speed railway design specification≫ (TB10621-2014). Its particle grading curves of five test results are shown in Figure 4. Figure 4 shows the test data have good consistency.

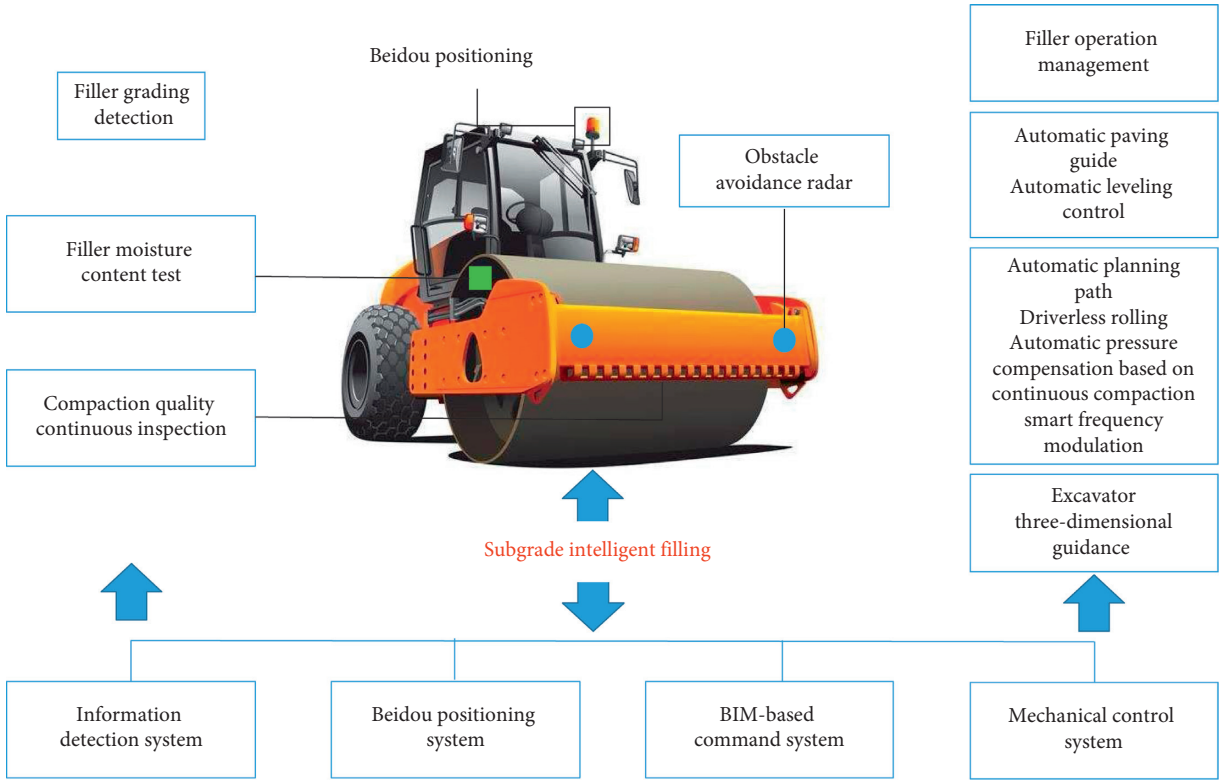

Figure 1: Schematic diagram of the intelligent road roller in the Gu'an section of Beijing-Xiong'an Railway.

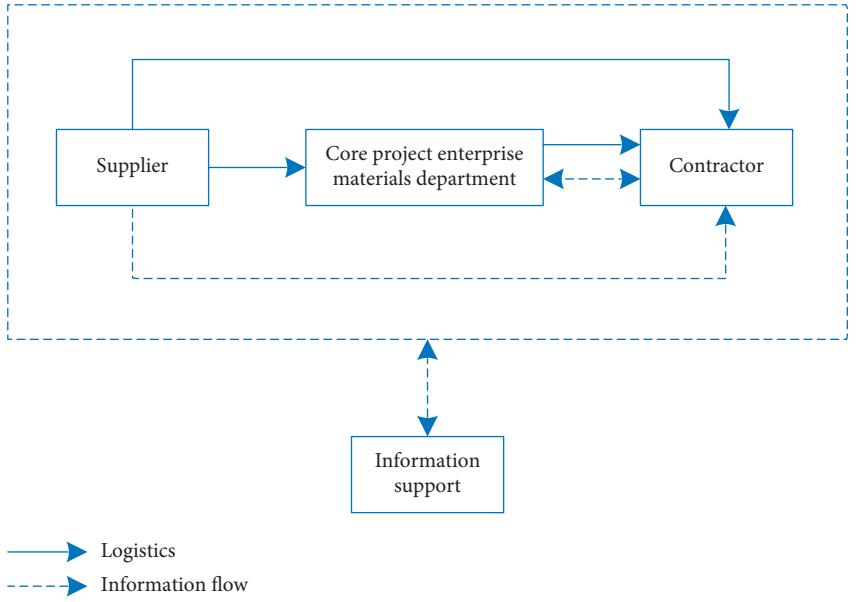

Figure 2: Project organizational logistics scheduling network.

3.1. Test Equipment. The vibratory compaction equipment adopts Sany Heavy Industry Vibratory Roller (No. SSR260C-6), the whole machine quality is 26.7 t, and its rated power is 180 kW. The weak vibration parameters: vibration frequency is 31 Hz, and vibration amplitude is 1.03 mm; the strong vibration parameters: vibration frequency is 27 Hz, and vibration amplitude is 2.05 mm. Based on a large number of actual projects in the early stage, it is found that the weak vibration is more conducive to the subgrade compaction after its filler is loosely laid and statically pressed. Consequently, the test adopts weak vibration conditions for research. At the same time, the data acquisition adopts 64-channel Donghua dynamic data acquisition equipment DH3823 and the acceleration sensor adopts Donghua three-way acceleration sensor 1C302 with a range of ±5.0 g. In order to ensure the fit between the collected signal and the original signal, the

Figure 3: Field test environment.

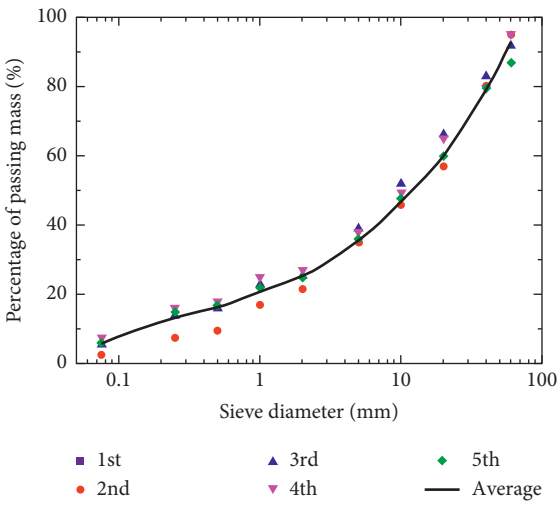

Figure 4: Particle grading curves of five tests.

sampling frequency of acceleration sensors was set to 2000 Hz. And all the data acquisition system and sensors were calibrated before the test.

3.2. Distribution of Acceleration Measuring Points in the Filler Material. The correct installation and embedment of sensors is decisive for the accuracy of test data. Before the sensors are buried, some work should be finished, as shown in Figure 5. At the same time, in order to study the vibration characteristics in different depths in the compaction process, the sensors are set on the vibratory wheel and its following five layers. The concrete distribution of acceleration measuring points in the filler material and the overall coordinate system in the field test are shown in Figures 6 and 7.

4. Test Results

In order to systematically analyse the propagation characteristics of vibration wave in the vertical direction, this paper will carry out the research from four aspects: time domain, frequency domain, joint time-frequency domain, and energy domain.

4.1. Propagation Characteristics of Peak Acceleration in the Vertical Direction. The duration of measured vibrational signal is nearly 10 seconds, so 10 second time-history curve is selected for analysis. The peak acceleration of vibration wave at each measuring point in the compaction process is shown in Figure 8.

Figure 8 shows that when vibration wave propagates from vibratory roller ⟶ filler surface ⟶ deep filler, the shape of peak acceleration is hyperbolic with the increase in buried depth and is also inversely proportional to buried depth. When the vibration wave propagates from frame ⟶ filler surface, the peak acceleration in the Z, Y, and X directions is, respectively, attenuated by 56.7%, 83.7%, and 85.1% and, respectively, attenuated by 94.5%, 98.6%, and 98.4% at a buried depth of 0.9 m, which is basically stable after that, and then, the vibration energy is nearly zero at a buried depth of 1.50 m in which the vibrational energy is, respectively, attenuated by 96.1%, 99.3%, and 98.7%. The above phenomenon may be caused by the dissipation of energy by the damping of the filler itself, and it can be seen that the critical depth of vibration energy propagation during the vibration compaction process is about 1.0 m. At the same time, at the interface of the filler, the vibration accelerations in different directions are stepped, which is mainly caused by the differences in physical and mechanical parameters between adjacent

(a) (b)

Figure 5: (a) Installation and embedment of sensors and (b) data acquisition in the field test.

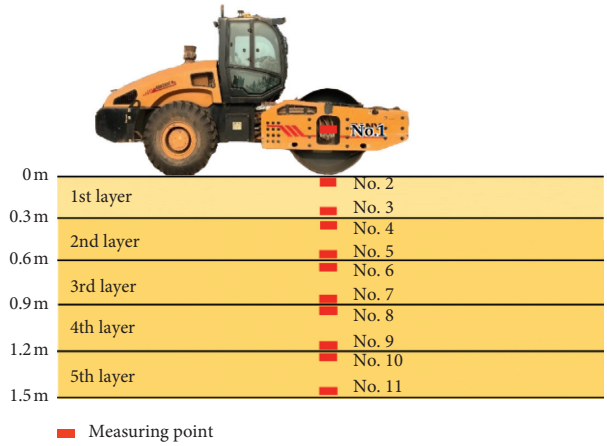

Figure 6: Acceleration measuring points in the filler material.

Figure 7: Schematic diagram of overall coordinate system in the field test.

filling material, especially the difference in wave impedance between the two sides of interface, which causes a large amount of reflection, transmission, and other scattering phenomenon at the interface, which weakens the downward propagation of vibration energy. Based on this, in order to analyze the influence of the filler interface on the vibration acceleration quantitatively, this paper assumes that the measurement point on the upper surface of each interface is used as the benchmark and uses the ratio

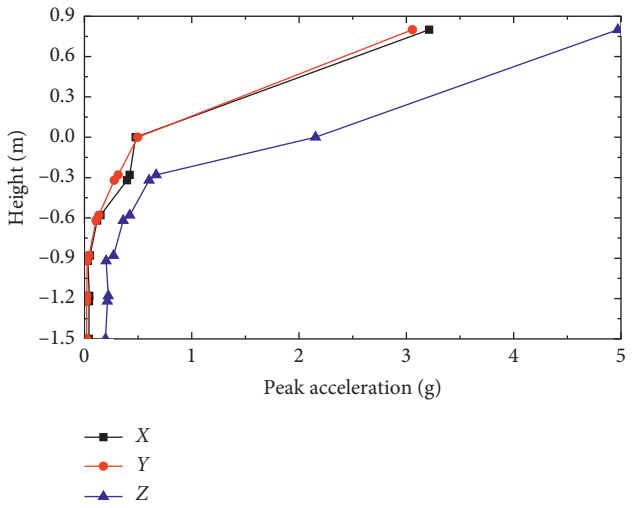

Figure 8: Distribution of peak acceleration at each measuring point in different directions.

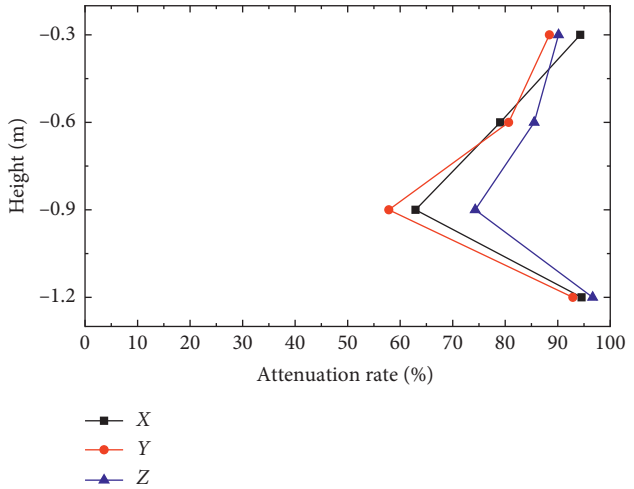

Figure 9: Attenuation of acceleration at different interfaces.

of the acceleration amplitude of the lower surface to the benchmark as acceleration peak attenuation percentage, and the result is shown in Figure 9.

Figure 9 shows that the attenuation characteristics of vibration acceleration in different directions with the increase in buried depth is basically consistent, showing a "side clock" shape, the attenuation in the X direction is more serious than the Y direction, and the Z direction is the smallest. At the same time, due to the increase in buried depth, the attenuation percentage at different interfaces decreases firstly, reaching minimum when the buried depth is 0.9 m, about 55%, and then gradually increases. The reason of the above phenomenon may be that the propagation depth of vibration energy is about 1.0 m, which can cause the secondary compaction within 1 m filling material in the compaction process, whose density and rigidity can gradually increase, and the compaction parts more than 1.0 m mainly depend on the inertial force generated by the vibration of upper filler and the upper heaped load. Consequently, the soil buried depth (0.6 m–0.9 m) realizes secondary compaction by vibration and that more than 0.9 m is compacted by inertia force and heaped load, and then, the acceleration attenuation is the largest, which is mainly due to the larger differences in the degree of compaction, and the density and stiffness of soil on both sides cause a large wave impedance and reflection of vibration energy, so the acceleration peak attenuation is small at the interface of 1.2 m buried depth (the soil within the range of 0.9 m–1.2 m/more than 1.2 m), which is for the reason that the soil density and stiffness on both sides of interface are basically consistent, so the reflection for vibration wave is small.

4.2. Propagation Characteristics of Acceleration Spectrum in the Vertical Direction. In order to research the propagation characteristics of acceleration spectrum in the vertical direction, the vertical acceleration data of #1, #3, #5, #7, #9, and #11 measuring points are selected for analysis. The results are shown in Figure 10.

Figure 10 shows that the frequency of fundamental wave in the #1 measuring point is near 21 Hz. When the vibration wave propagates in the filling material, the first harmonic is near 42 Hz, the second harmonic is near 63 Hz, the third harmonic is near 84 Hz, the fourth harmonic is near 105 Hz, and the fifth harmonic is stable at 130 Hz. At the same time, the dominant frequency of first harmonic is basic consistent, but that of the other harmonics gradually increase, as shown in Figure 11.

The above phenomenon may be for the reason that the density and stiffness of the filler gradually increase with the increase in the buried depth, which causes the high-frequency component of the vibration wave to gradually increase and the low-frequency component to appropriately lower, thereby causing the main frequency of the harmonic to gradually change to a high frequency, and the ratio of the amplitude of the harmonic wave to the fundamental wave is also gradually increasing.

4.3. Propagation Characteristics of Vibration Wave Energy in the Vertical Direction. In order to accurately describe the propagation characteristics of vibration wave energy in the vertical direction as shown in Figure 12, the measured acceleration time-history curves at the monitoring points #1–#11 are selected to calculate the acceleration marginal spectrum at different depths, and the calculation results are shown in Figures 13 and 14.

Figures 13 and 14 show that the vibration wave energy is mainly concentrated near 10–30 Hz in the vibratory roller, which is basically consistent with the fundamental wave frequency. However, the peak values of marginal spectrum gradually change from one to two. The vibration wave energy is mainly concentrated near 30–50 Hz and 50–100 Hz, and the energy of signal gradually decreases with the increase in buried depth. The test phenomenon fully shows that the vibration energy in the frequency appears as large change with the increase in buried depth, and the percentage of higher harmonic energy in the total energy gradually increases. When the vibration energy is transmitted from the roller to the surface of the filler, the vibration energy is dissipated, and the transmission efficiency is low; therefore, how to improve the energy transfer efficiency is essential for energy saving and efficiency improvement.

4.4. Three-Dimensional Propagation Characteristics of Vibration Wave in Vertical Direction. In order to fully describe the propagation characteristics of vibration wave in the vertical direction, the Hilbert–Huang spectrum at different buried depths is calculated by using Hilbert–Huang transform.

4.4.1. Introduction to Hilbert–Huang Transform. The HHT transform is an autoadaptive time-frequency analysis method proposed by Norden E. Huang in 1998 for nonlinear and unstable signal processing, which mainly includes empirical mode decomposition and Hilbert spectrum analysis [14]. The EMD algorithm (Formula (1)) can decompose the complex vibration wave signal into multiple intrinsic mode functions IMF, and the distribution law of time-frequency-energy of each IMF signal can be obtained by HHT transform (Formula (2)), that is, Hilbert spectrum, and it is worth noting that the relevant parameters in equations (1) and (2) are found in [15]:

$$c_j(t) = \frac{1}{N}\sum_{i=1}^{N} c_{ij}(t). \tag{1}$$

$$H(w,t) = \mathrm{Re}\sum_{i=1}^{n+1} a_i(t)\cdot e^{j\int w_i(t)dt}. \tag{2}$$

4.4.2. Empirical Mode Decomposition of Vibration Wave. The measured acceleration time-history is selected to introduce. First, EMD is performed on the original wave, and several IMF signals and one residual moisture are obtained. IMF4, IMF5, and IMF6 are selected to illustrate the frequency component of measured acceleration time-history, as shown in Figures 15–17.

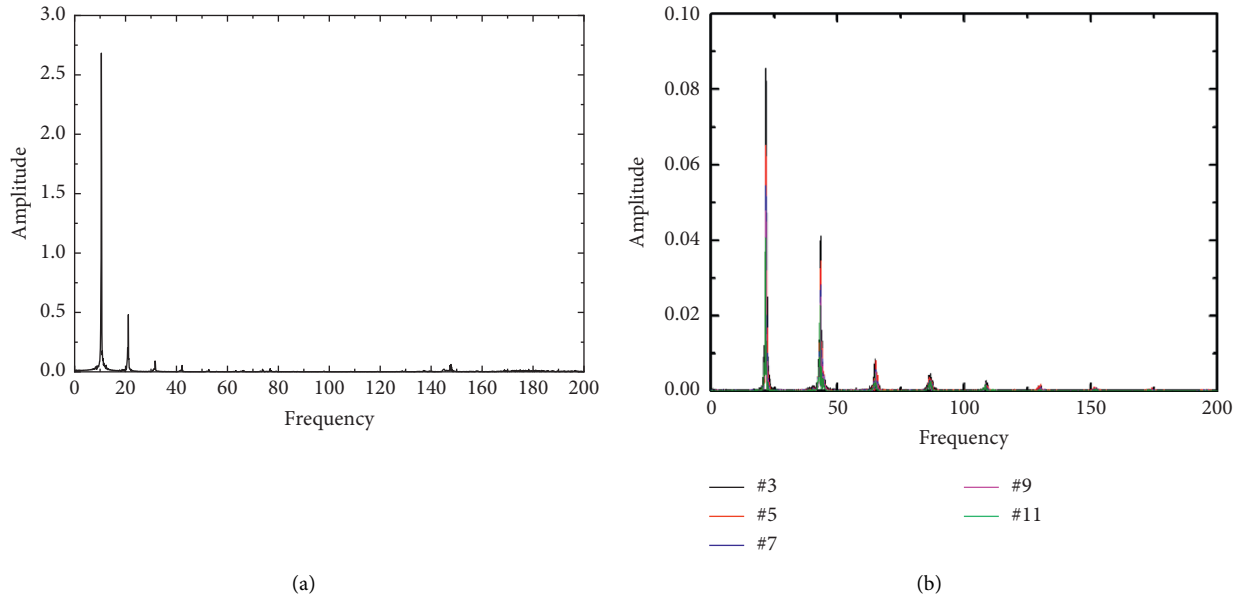

Figure 10: Distribution of Fourier spectrum in vertical direction: (a) Fourier spectrum of #1 measuring point; (b) Fourier spectrum of #3, #5, #7, #9, and #11 measuring points.

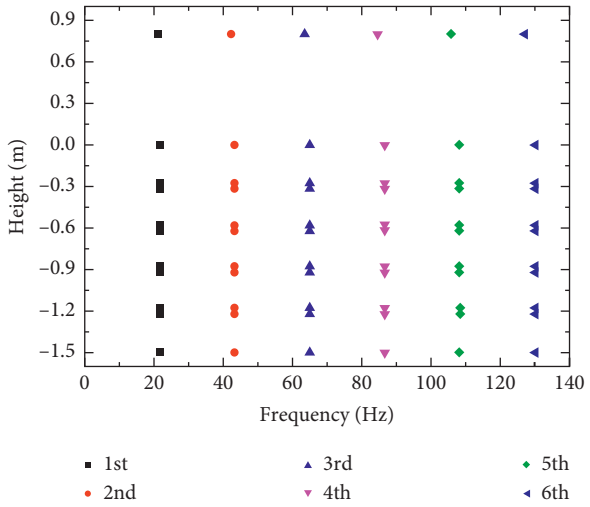

Figure 11: Evolution law of harmonic frequency along buried depth.

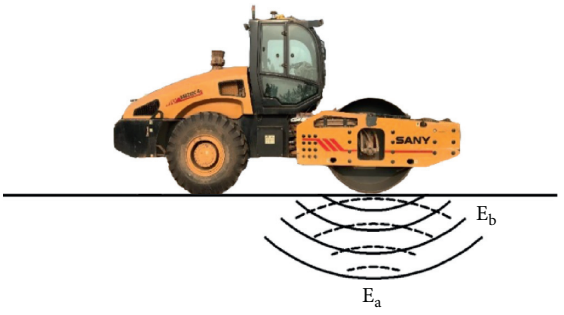

E_a — Compaction energy produced by vibratory roller

E_b — Compaction energy returned to vibratory roller

Figure 12: Energy interaction between vibratory roller and surface of filling material.

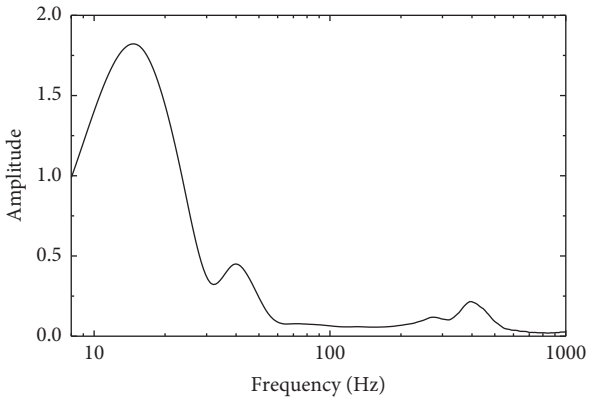

Figure 13: Distribution of vibration wave energy in vibrational wheel.

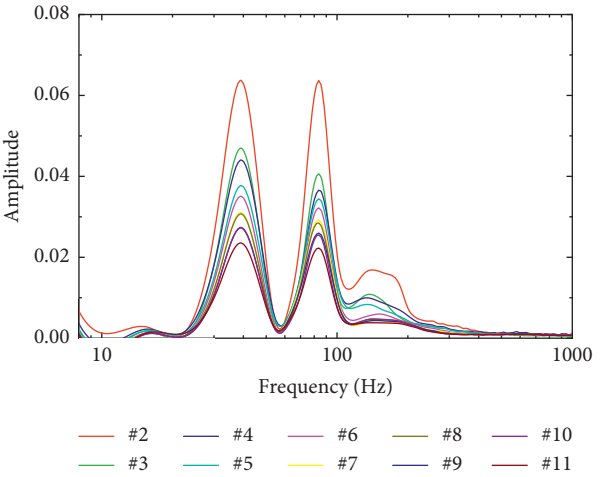

Figure 14: Distribution of vibration wave energy in different buried depths.

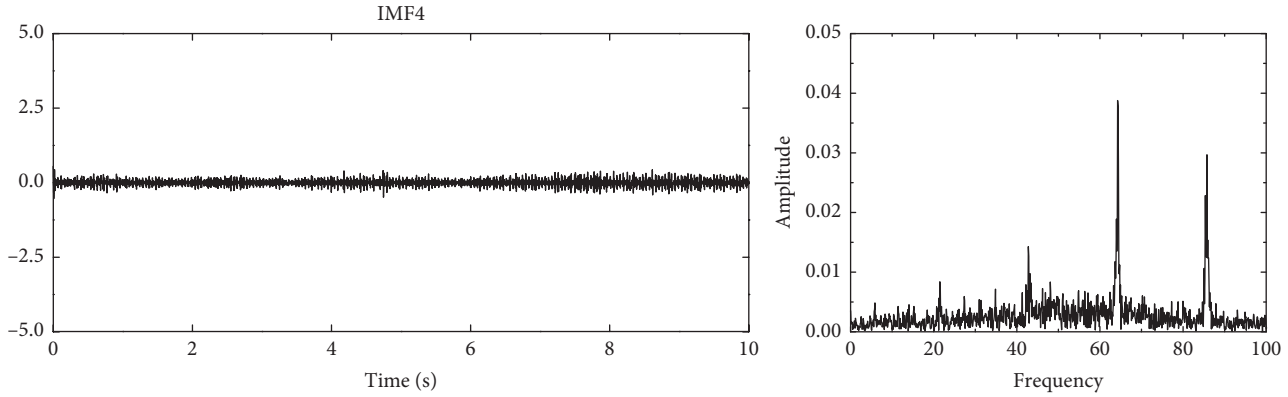

Figure 15: IMF4 and its FFT spectrum.

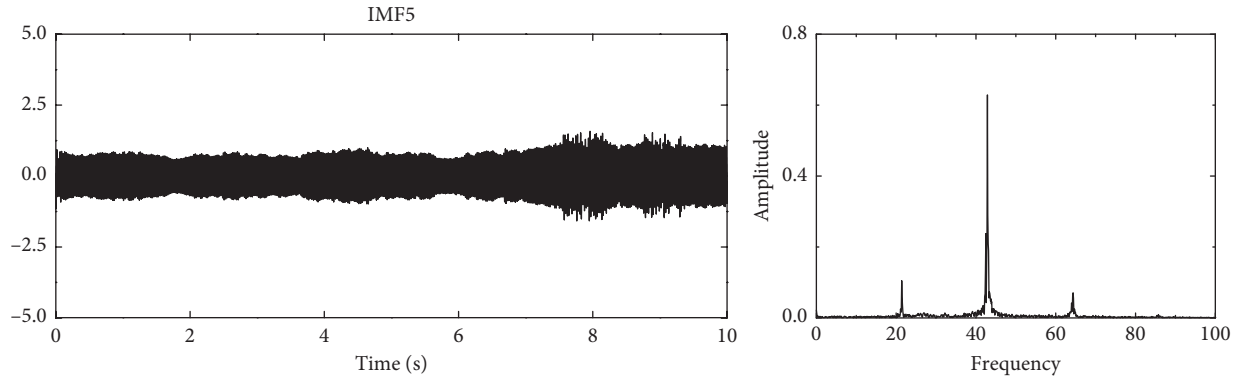

Figure 16: IMF5 and its FFT spectrum.

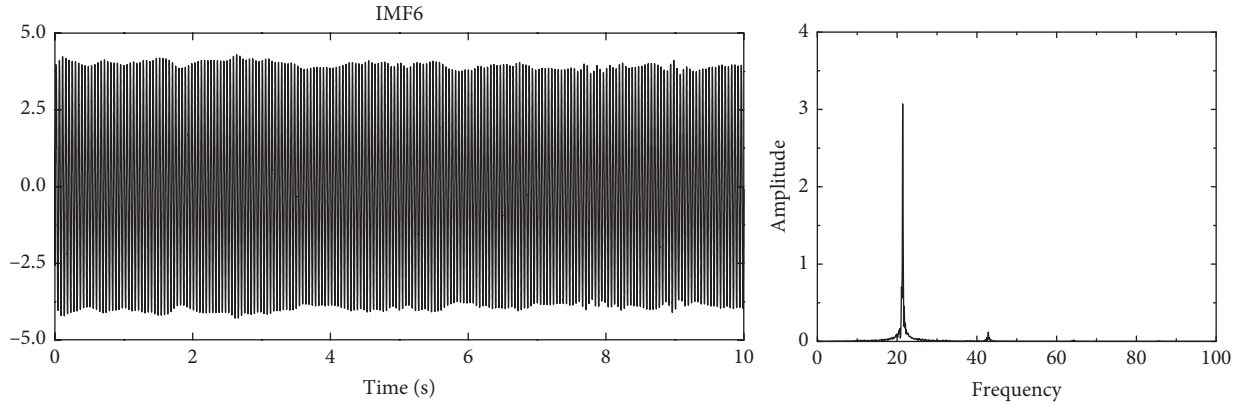

Figure 17: IMF6 and its FFT spectrum.

Among the abovementioned IMF components, the peak value of IMF6 is biggest. Its waveform and dominant frequency are consistent with that of original signal; IMF5 dominant frequency is the closest to the first harmonic. The frequencies with the largest amplitude of IMF4 are basically consistent with that of second and third harmonic waves of original vibration signal, and the remaining components are high-frequency or low-frequency interference signals. Therefore, the waveform of wheel is composed of IMF6, IMF5, and IMF4. To some extent, EMD can identify the fundamental and harmonic components of vibration signals and remove the mechanical and environmental noise interference.

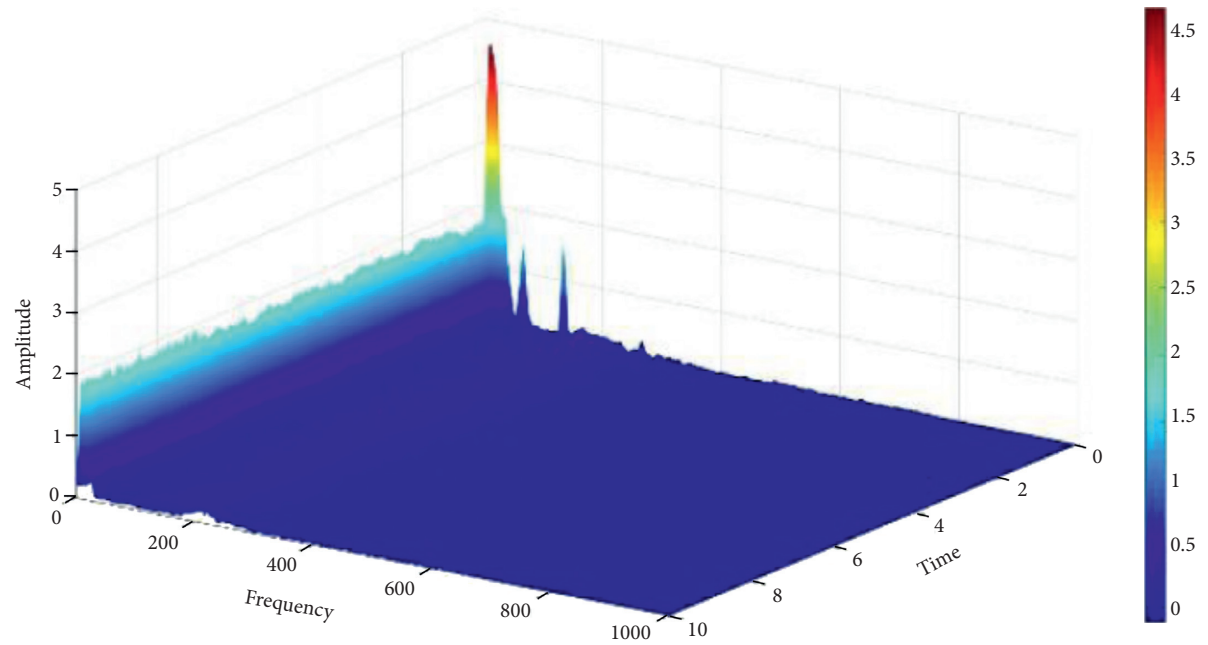

(a)

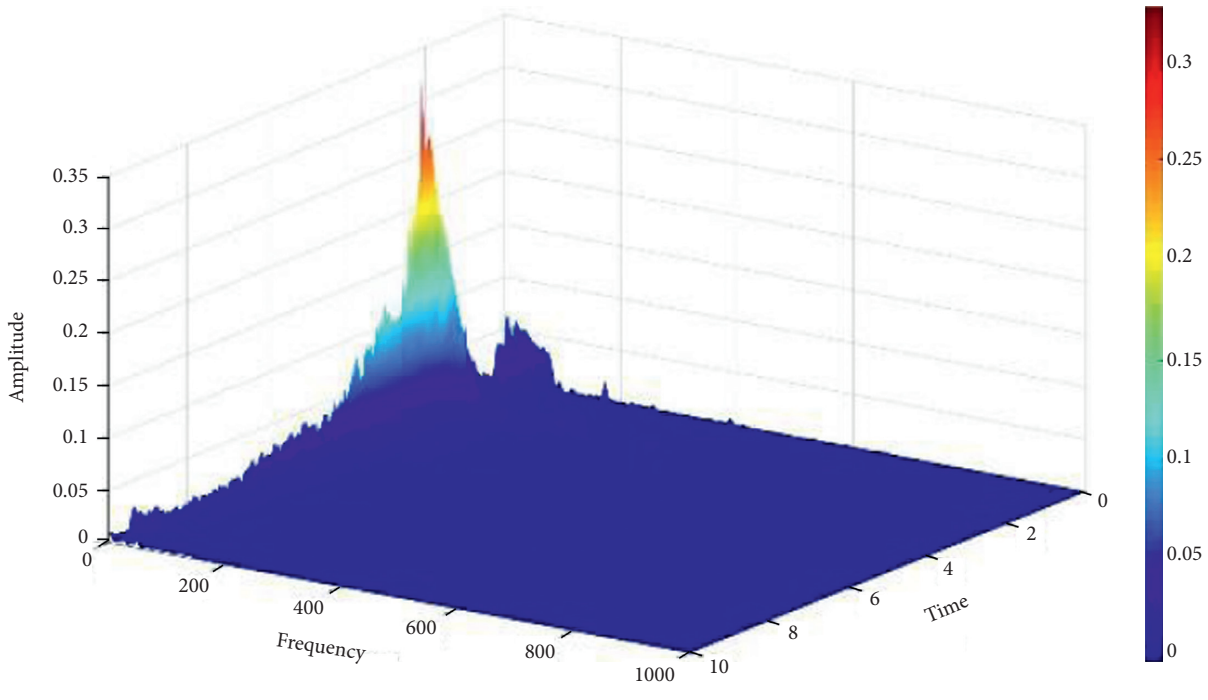

(b)

Figure 18: Continued.

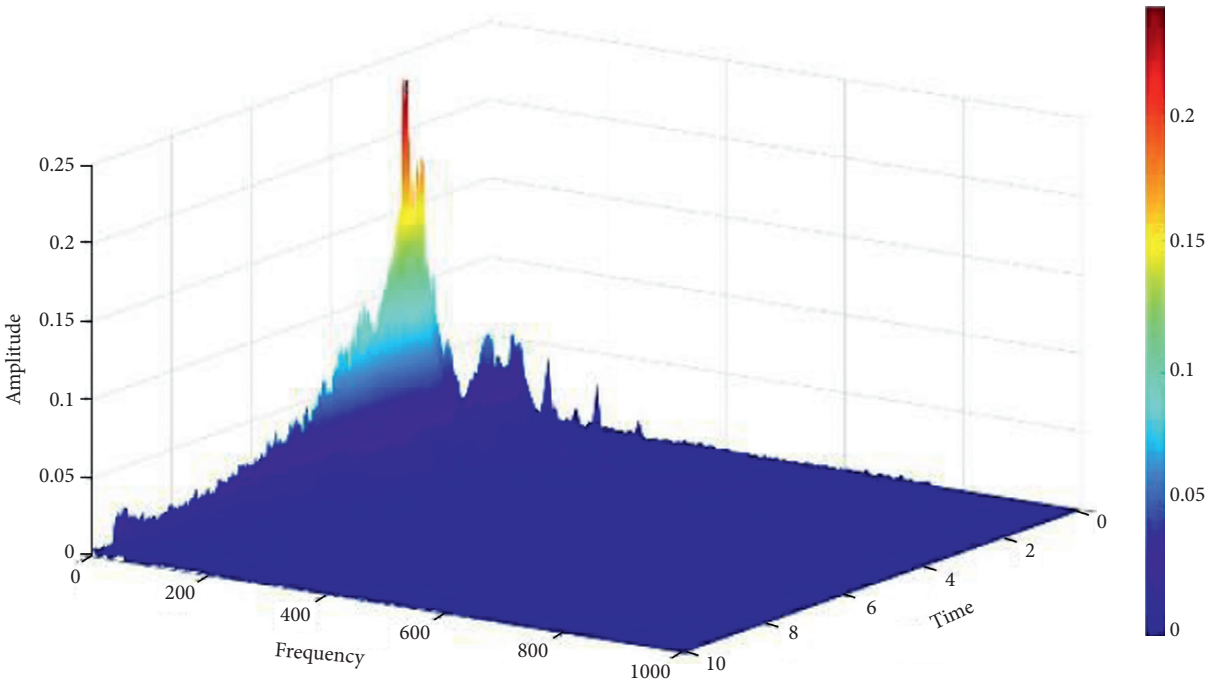

(c)

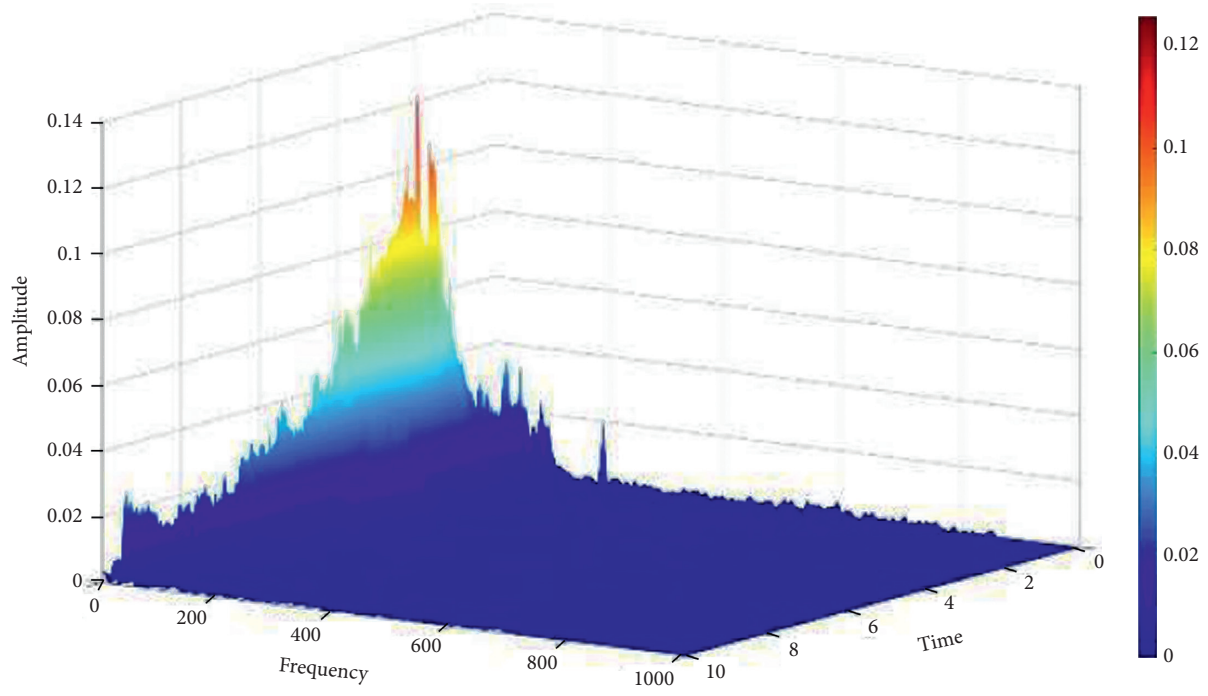

(d)

Figure 18: Continued.

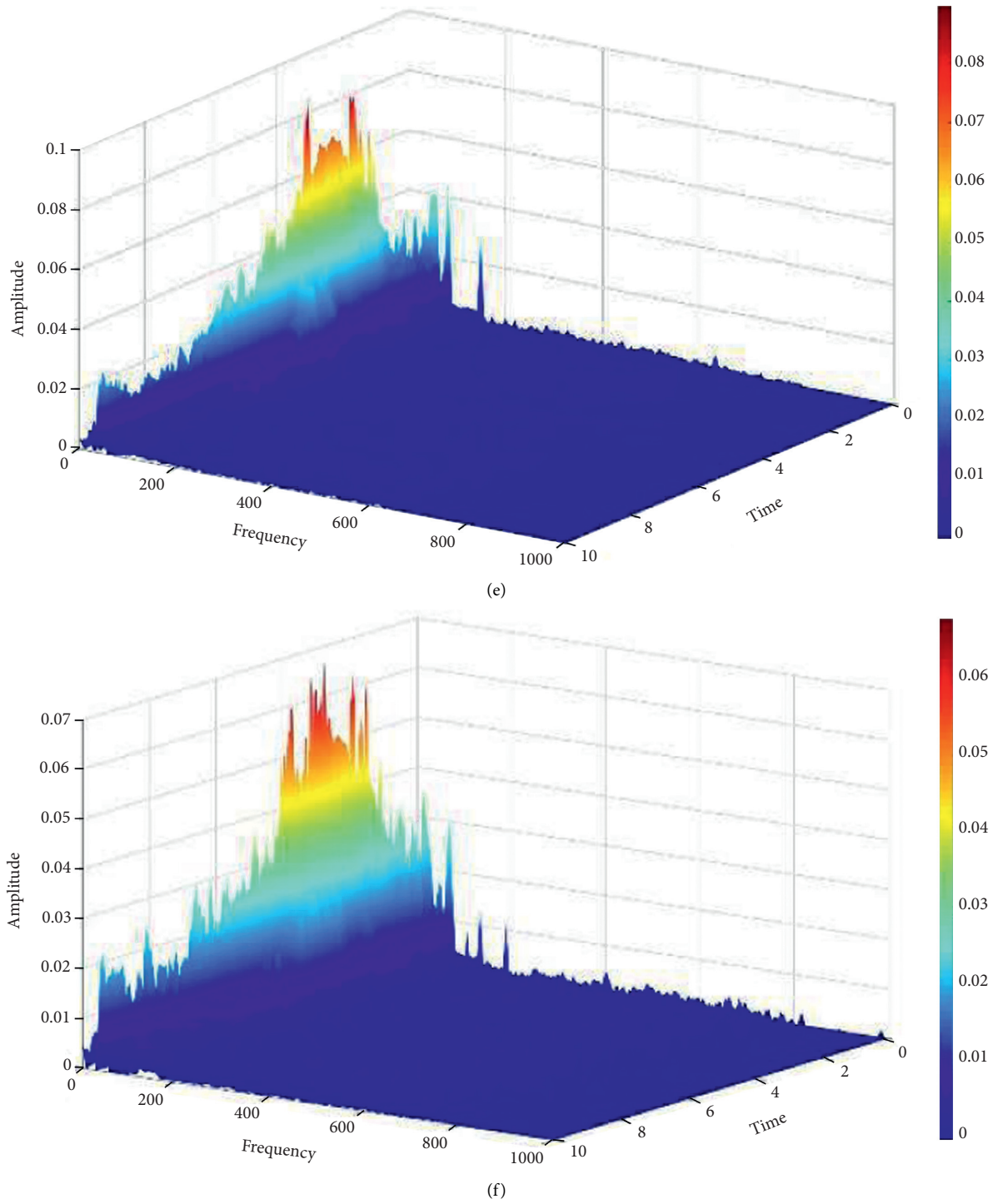

Figure 18: Hilbert–Huang spectrums at points (a) #1, (b) #3, (c) #5, (d) #7, (e) #9, and (f) #11.

4.4.3. Hilbert–Huang Spectrum of Vibrational Wave. In order to systematically analyze the propagation characteristics of Hilbert spectrum in the different buried depths, this paper selects the Hilbert–Huang spectrums of #1, #3, #5, #7, #9, and #11 measuring points, as shown in Figure 18.

Figure 18 shows that the vibration energy in the vibratory roller is distributed averagely in the compaction process, and the corresponding frequency is between 10 Hz and 30 Hz. The vibration energy in the subgrade filling mainly concentrates between $T = 2.0$ s and $T = 4.0$ s, and the corresponding frequency is between 30 Hz and 100 Hz. Therefore, the effective compaction time is two seconds. Consequently, the Hilbert spectrum of vibration wave signal can comprehensively and systematically reflect the spectral characteristics and time-domain characteristics of the signal at any time.

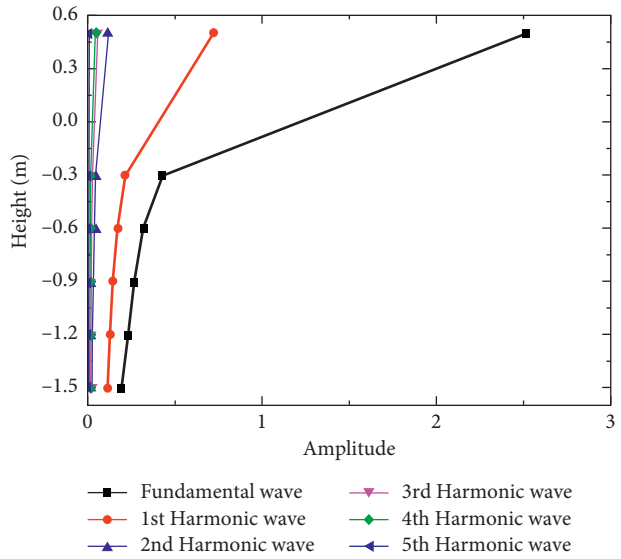

Figure 19: Different harmonic wave amplitudes in different buried depths.

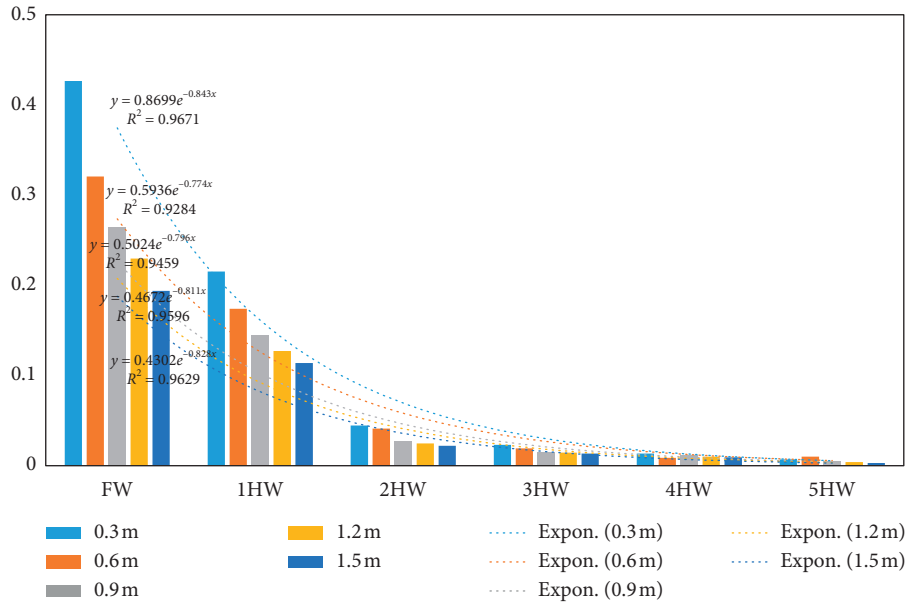

Figure 20: Concrete functional relationship among different amplitudes of harmonics.

4.5. Propagation Characteristics of Vibration Harmonic Wave in the Vertical Direction. In order to comprehensively study the propagation characteristics of vibration harmonic wave in the vertical direction, the frequency and amplitude of first, second, third, fourth, and fifth harmonic waves in the vertical direction are selected, as shown in Figures 19 and 20.

Figure 19 shows that, with the increase in buried depth, the amplitude of every harmonic gradually decreases. At the same time, the amplitude of fundamental, primary, secondary, until fifth harmonics decreases exponentially with the order of harmonic (R^2>0.9), and the attenuation models are shown in Figure 20. The concrete functional relationship among different amplitudes of harmonics can be summarized, as shown in $y = Ae^{-BX}$; in formula, A and B represent the coefficient, X represents the order of harmonic, and Y represents the amplitude of harmonic when its order is X.

5. Conclusion

Aiming at the shortages, one typical subgrade located at the Gu'an station of Beijing-Xiong'an city railway is selected to research and finish the field tests, and some research results are shown as follows.

First, when the vibration wave propagates from the vibratory roller ⟶ surface of filling material⟶different buried depths of filling material, the peak acceleration of vibration wave gradually decreases and is hyperbolic distribution approximately. At the same time, the sensitive of

attenuation is shown as follows: $Z<X \approx Y$, and the critical depth of vibration energy propagation is about 1.0 m. At the same time, the peak acceleration of vibration wave at the interface of different filling material layers exists in steps and is "side clock" distribution approximately with the increase in buried depth.

Second, in the propagation process, with the increase in buried depth, the amplitude of fundamental, primary, secondary, until fifth harmonics decreases exponentially ($R^2>0.9$), and the concrete functional relationship among different amplitudes of harmonics can be summarized as $y = Ae^{-BX}$.

Third, the vibration energy is mainly concentrated near 10–30 Hz in the vibratory roller, but when the vibration wave propagates from vibratory roller ⟶ filling material, the vibration energy gradually decreases with the increase in depth, and the marginal spectrum gradually changes from one peak to two peaks that 30–50 Hz and 50–100 Hz; fourth, the waveform of vibratory roller is composed of IMF6, IMF5, and IMF4. At the same time, EMD can identify the fundamental and harmonic components of vibration signals and remove the mechanical and environmental noise interference. The vibration energy in the vibrational wheel is distributed averagely in the compaction process, and the effective compaction time is two seconds, which will be helpful for optimizing the compaction quality control models of railway subgrade.

Data Availability

The data used to support the findings of this study are available from the corresponding author upon request.

Conflicts of Interest

The authors declare that there are no conflicts of interest regarding the publication of this article.

Acknowledgments

This study was supported in part by the National Key Research and Development Plan (no. 2018YFE0207100), Natural Science Foundation of China (Contract no. 41731288), Sichuan Provincial Science and Technology Support Project (nos. 18MZGC0186, 18MZGC0247, and 2018JY0549), China National Railway Group Co. Ltd Scientific Research Project (nos. SY2016G003, N2019G002, and P2019T001), China Academy of Railway Sciences Corporation Limited Research and Development fund (no. 2019YJ026), 2017–2019 Young Elite Scientist Sponsorship Program by CAST, 2019 Young Top Talent Sponsorship Program of China Ten thousand people plan (no. 2019YJ300), 2018 Sichuan province Ten thousand people plan, Nanchang Railway Bureau Scientific Research Project (no. 20171106), and China Railway Eryuan Engineering Group Co. Ltd Scientific Research Project (no. KYY2019145 (19-20)).

References

[1] R. Anderegg and K. Kaufmann, "Intelligent compaction with vibratory rollers: feedback control systems in automatic compaction and compaction control," *Transportation Research Record: Journal of the Transportation Research Board*, vol. 1868, no. 1, pp. 124–134, 2004.

[2] L. Dong, D. Sun, X. Li, J. Ma, L. Zhang, and X. Tong, "Interval non-probabilistic reliability of surrounding jointed rockmass considering microseismic loads in mining tunnels," *Tunnelling and Underground Space Technology*, vol. 81, pp. 326–335, 2018.

[3] M. A. Mooney, *Intelligent Soil Compaction Systems*, Transportation Research Board, Washington, D. C., USA, 2010.

[4] D. Adam, "Roller-integrated continuous compaction control (CCC) Technical Contractual Provisions & Recommendations," *Design and Construction of Pavements and Rail Tracks*, vol. 10, pp. 111–138, 2007.

[5] S. A. Kumar, R. Aldouri, S. Nazarian et al., "Accelerated assessment of quality of compacted geomaterials with intelligent compaction technology," *Construction and Building Materials*, vol. 113, pp. 824–834, 2016.

[6] D. Liu, M. Lin, and S. Li, "Real-time quality monitoring and control of Highway compaction," *Automation in Construction*, vol. 62, pp. 114–123, 2016.

[7] L. Dong, X. Tong, X. Li, J. Zhou, S. Wang, and B. Liu, "Some developments and new insights of environmental problems and deep mining strategy for cleaner production in mines," *Journal of Cleaner Production*, vol. 210, pp. 1562–1578, 2019.

[8] M. A. Mooney and R. V. Rinehart, "Field monitoring of roller vibration during compaction of subgrade soil," *Journal of Geotechnical and Geoenvironmental Engineering*, vol. 133, no. 3, pp. 257–265, 2007.

[9] J. Pistrol, S. Villwock, W. Völkel, F. Kopf, and D. Adam, "Continuous compaction control (CCC) with Oscillating rollers," *Procedia Engineering*, vol. 143, pp. 514–521, 2016.

[10] M. Thompson and D. White, "Field calibration and Spatial analysis of compaction-monitoring technology measurements," *Journal of the Transportation Research Board*, vol. 2004, pp. 69–79, 2007.

[11] T. S. Yoo, *A Theory for Vibratory Compaction of Soils*, pp. 44–52, State university of New York at Buffalo, Buffalo, New York, USA, 1975.

[12] C. Herrera, P. Alves Costa, and B. Caicedo, "Numerical modelling and inverse analysis of continuous compaction control," *Transportation Geotechnics*, vol. 17, pp. 165–177, 2018.

[13] J. Xu, "Research on network structure and operation of logistics organization," Ph.D. thesis, Beijing Jiaotong University, Beijing, China, 2007.

[14] N. E. Huang, Z. Shen, S. R. Long et al., "The empirical mode decomposition and the Hilbert spectrum for nonlinear and non-stationary time series analysis," *Proceedings of the Royal Society of London. Series A: Mathematical, Physical and Engineering Sciences*, vol. 454, no. 1971, pp. 903–995, 1998.

[15] N. E. Huang, M.-L. C. Wu, S. R. Long et al., "A confidence limit for the empirical mode decomposition and Hilbert spectral analysis," *Proceedings of the Royal Society of London. Series A: Mathematical, Physical and Engineering Sciences*, vol. 459, no. 2037, pp. 2317–2345, 2003.